Physics Letters B 747 (2015) 129–134

Contents lists available at ScienceDirect

Physics Letters B

www.elsevier.com/locate/physletb

Hypernuclear production cross section in the reaction of ^{6}Li + ^{12}C at 2 *A* GeV

C. Rappold [a,b,*], T.R. Saito [a,c,d,e], O. Bertini [a,c], S. Bianchin [a], V. Bozkurt [a,f], E. Kim [a,g], M. Kavatsyuk [h], Y. Ma [a,c], F. Maas [a,c,d], S. Minami [a], D. Nakajima [a,i], B. Özel-Tashenov [a], K. Yoshida [a,d,j], P. Achenbach [c], S. Ajimura [k], T. Aumann [l,a], C. Ayerbe Gayoso [c], H.C. Bhang [g], C. Caesar [l,a], S. Erturk [f], T. Fukuda [n], B. Göküzüm [a,f], E. Guliev [h], J. Hoffmann [a], G. Ickert [a], Z.S. Ketenci [f], D. Khaneft [a,c], M. Kim [g], S. Kim [g], K. Koch [a], N. Kurz [a], A. Le Fèvre [a,m], Y. Mizoi [n], L. Nungesser [c], W. Ott [a], J. Pochodzalla [c,d], A. Sakaguchi [j], C.J. Schmidt [a], M. Sekimoto [o], H. Simon [a], T. Takahashi [o], G.J. Tambave [h], H. Tamura [p], W. Trautmann [a], S. Voltz [a], C.J. Yoon [g]

[a] *GSI Helmholtz Centre for Heavy Ion Research, Planckstrasse 1, 64291 Darmstadt, Germany*
[b] *Justus-Liebig-Universität Giessen, Heinrich-Buff-Ring 16, 35392 Giessen, Germany*
[c] *Johannes Gutenberg-Universität Mainz, J.J. Becherweg 40, 55099 Mainz, Germany*
[d] *The Helmholtz Institute Mainz (HIM), J.J. Becherweg 40, 55099 Mainz, Germany*
[e] *Iwate University, Morioka, Iwate 020-8550, Japan*
[f] *Nigde University, 51100 Nigde, Turkey*
[g] *Seoul National University, Gwanakro Sillim-dong, Gwanak-gu, Seoul 151-747, Republic of Korea*
[h] *KVI, University of Groningen, Zernikelaan 25, NL-9747 AA Groningen, The Netherlands*
[i] *The University of Tokyo, 7-3-1 Hongo, Bunkyo-ku, Tokyo 113-0033, Japan*
[j] *Osaka University, 1-1 Machikaneyama, Toyonaka, Osaka 560-0043, Japan*
[k] *Research Centre for Nuclear Physics (RCNP), 10-1 Mihogaoka, Ibaraki, Osaka 567-0047, Japan*
[l] *Technische Universität Darmstadt, 64289 Darmstadt, Germany*
[m] *SUBATECH, La Chantrerie, 4 rue Alfred Kastler, BP 20722, 44307 Nantes, France*
[n] *Osaka Electro-Communication University, Hatsu-cho 18-8, Neyagawa, Osaka 572-8530, Japan*
[o] *KEK, 1-1 Oho, Tsukuba, Ibaraki 305-0801, Japan*
[p] *Tohoku University, 6-3 Aoba Aramaki Aoba Sendai, Miyagi 980-7875, Japan*

ARTICLE INFO

Article history:
Received 23 December 2014
Received in revised form 17 April 2015
Accepted 25 May 2015
Available online 27 May 2015
Editor: V. Metag

Keywords:
Hypernuclei
Production cross section
Yield ratio
Relativistic energy
Heavy ion collision

ABSTRACT

Hypernuclear production cross sections have been deduced for the first time with induced reaction of heavy ion beam on fixed target and by means of the invariant mass method by the HypHI Collaboration exploiting the reaction of ^{6}Li + ^{12}C at 2 *A* GeV or $\sqrt{s_{NN}} = 2.70$ GeV. A production cross section of 3.9 ± 1.4 μb for $^{3}_{\Lambda}$H and of 3.1 ± 1.0 μb for $^{4}_{\Lambda}$H respectively in the projectile rapidity region was inferred as well as the total production cross section of the Λ hyperon was measured and found to be equal to 1.7 ± 0.8 mb. A global fit based on a Bayesian approach was performed in order to include and propagate statistical and systematic uncertainties. Production ratios of $^{3}_{\Lambda}$H/$^{4}_{\Lambda}$H, $^{3}_{\Lambda}$H/Λ and $^{4}_{\Lambda}$H/Λ were included in the inference procedure. The strangeness population factors S_3 and S_4 of $^{3}_{\Lambda}$H and $^{4}_{\Lambda}$H respectively were extracted. In addition, the multiplicities of the Λ hyperon, $^{3}_{\Lambda}$H, and $^{4}_{\Lambda}$H together with the rapidity and transversal momentum density distributions of the observed hypernuclei were extracted and reported.

1. Introduction

Reactions between complex nuclei have been a powerful tool to investigate subatomic structures as well as chemical properties of nuclear matter. In relativistic heavy ion collisions, the gen-

* Corresponding author.
E-mail addresses: c.rappold@gsi.de (C. Rappold), t.saito@gsi.de (T.R. Saito).

http://dx.doi.org/10.1016/j.physletb.2015.05.059

eral feature of the reaction is well described by the participant-spectator concept [1]: the participant nucleons in the overlap region between the two colliding nuclei enter in collision, while the spectator nucleons in the non-overlapping regions pass by each other without interacting. Many hadrons are produced in the hot participant zone, and widely distributed between the target and projectile rapidities [2,3]. Hadrons from this hot participant zone may interact with the spectators and can be captured by the spectator fragments [4,5]. The spectator fragments or produced hadrons can be excited to unstable particles and later decay to their ground states by emitting particles and/or γ-rays.

Laying the nucleon–nucleon Λ threshold at 1.58 GeV [6,7], the wide rapidity distribution of produced Λ-hyperons can overlap with those of the projectile and the target spectators. Thus, the Λ-hyperon can be combined to a spectator fragment, and a Λ-hypernucleus can be produced in projectile or target rapidity regions [8]. The experimental viability of the hypernuclear spectroscopy is assessed by the order of magnitude of the production cross section. Additionally, their production cross section is a crucial physical observable which can provide more global understanding of the heavy ion collisions involving both participants and spectators at intermediate energies.

The first attempt to produce hypernuclei in the projectile rapidity regime was made with ^{16}O beams at 2.1 A GeV on a polyethylene target [9] estimating a hypernuclear cross section of the order of µb. Later, in the reaction of a beam of ^{4}He at 3.7 A GeV and ^{7}Li at 3.0 A GeV on a polyethylene target the cross section of $^{4}_{\Lambda}$H of 0.4 µb was estimated [10,11]. Those first experimental estimations of the production cross section do not agree on the magnitude of the cross sections, and a clear conclusion could not be stated due to the small number of light hypernuclei observed in both cases. Those rough estimations were then compared with the theoretical calculations within a simple coalescence model [8,12–14]. However, the identification of produced hypernuclei was ambiguous since the invariant mass of the final states was not measured. Subsequently, central collisions of platinum projectiles at 11.5 A GeV/c on a gold target were used to produce and identify $^{3}_{\Lambda}$H (hypertriton) and to estimate the upper limit for the observation of $^{4}_{\Lambda}$H hypernuclei [15]. Recently, the STAR Collaboration used gold–gold collisions at $\sqrt{s_{NN}} = 200$ GeV to study hypertriton and anti-hypertriton [16,17], followed by the observation of the ALICE Collaboration of those both hypernuclei in the lead–lead collisions at $\sqrt{s_{NN}} = 2.76$ TeV [18,19]. Those experiments observed hypernuclei in the mid-rapidity region and in ultra-relativistic heavy ion collisions, where the hypernuclei are formed by sudden hadronization at the chemical freeze-out. Therefore they provide information on the production mechanism in the hot participant zone that is described theoretically by statistical hadronization models [20,21].

The hypernuclear production at intermediate energy has also been studied theoretically in addition to the statistical models of the ultra-relativistic energy, by employing a phase space coalescence model [22,23] and Fermi-break up of excited hypernuclear spectators [24]. Yet the extremely scarce experimental data currently available do not restrain those models. One has to also notice that first theoretical work from [8,12–14] and updated calculations [22–24] differ by order of magnitude on the prediction of the hypernuclear production cross sections.

Recently, the HypHI Collaboration has observed the production of light hypernuclei, $^{3}_{\Lambda}$H and $^{4}_{\Lambda}$H in a reaction with ^{6}Li projectiles impinging on a graphite (^{nat}C) target [25]. The production cross section of $^{3}_{\Lambda}$H and $^{4}_{\Lambda}$H should provide information on the production mechanism of hypernuclear spectators since hypernuclear matter is expected to stem from the participant and spectator regions. Performing hypernuclear spectroscopy in the spectator region has also an advantage of a better observation efficiency

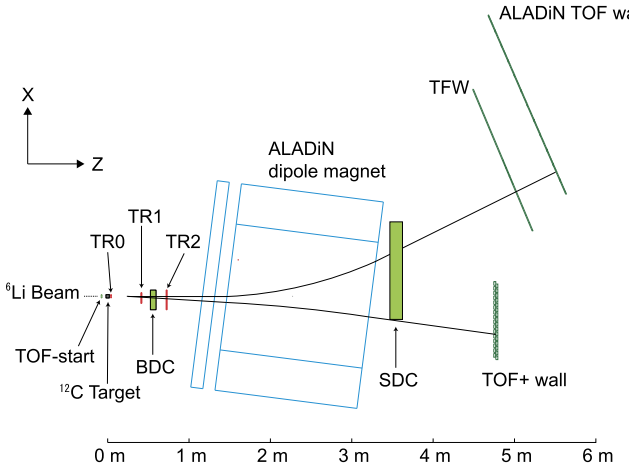

Fig. 1. Layout of the experimental setup.

compared to the heavy ion experiment studying the mid-rapidity region. During the data collection, over 3.5 integrated days, the final estimation of the integrated luminosity is 0.054 pb^{-1}, in which several hundreds of hypernuclei were observed. We have deduced the cross section of $^{3}_{\Lambda}$H and $^{4}_{\Lambda}$H for the first time with unique identification of those hypernuclei produced by ^{6}Li projectiles.

In this Letter, we provide the information on the cross section of these hypernuclei, together with the Λ production cross section and the yield ratio of the different species. The *strangeness population factors* S_3 and S_4 are reported. The multiplicity per collision of those species and the observed hypernuclear rapidity in the center-of-mass system, $y0 = y/y_{\mathrm{CM}} - 1$, and transversal momentum, Pt, density distribution are also presented.

2. Experimental apparatus

The experiment was performed with ^{6}Li projectiles at 2 A GeV with an intensity of 3×10^{6} ions per second bombarding on a graphite (^{nat}C) target with a thickness of 8.84 g/cm^2. As discussed in [25], the experimental apparatus, shown in Fig. 1, consisted of three tracking stations of scintillating fiber detector arrays (*TR0, TR1, TR2*) and two drift chambers (*BDC, SDC*) for the displaced vertex measurement. As well, three scintillating hodoscope walls (*TOF+, TFW, ALADiN TOF*) were appended to the tracking systems for tracking, energy loss and time-of-flight measurements of charged particles across a large acceptance dipole magnet. The tracking system for vertexing was placed in front of the dipole magnet around the expected decay volume of hypernuclei, while the *SDC* drift chamber was mounted behind the magnet. Two detached detection branches consisting of *TOF+* and *TFW & ALADiN TOF* hodoscope walls were situated behind the magnet as such to measure separately positively and negatively charged particles, respectively.

At the trigger level, the event topology was selected in order to record potential events containing a Helium isotope and a π^- stemming from a displaced vertex. The displaced vertex trigger used the information of *TR0*, *TR1* and *TR2* fiber detector arrays that were placed around the decay volume of hypernuclei and Λ hyperons. The Helium isotope trigger used the time-over-threshold measurement of the energy loss from the *TOF+* hodoscope wall dedicated solely for the positively-charge particles and fragments. The π^- trigger involved the hit detection on the *TFW* hodoscope wall dedicated exclusively for π^- detection behind the dipole magnet. This topological combination at hardware level was exploited in order to cope with the large difference of magnitude between the hypernuclear production cross section and the total reaction cross section. During the trigger design, a difference of

seven order of magnitude was considered, which was confirmed by the cross section and multiplicity estimations reported later in this Letter.

The particle identification was based on the track reconstruction across the magnet, the measurements of the time-of-flight, and the energy deposit with the hodoscope walls. The four-vectors of the detected particles and fragments were then deduced. The invariant mass of the final states of interest was calculated and a lifetime estimation was inferred from the observed decay vertex position after the decay vertex finding. Invariant mass distributions and the estimated lifetime values of Λ, ${}^{3}_{\Lambda}\mathrm{H}$ and ${}^{4}_{\Lambda}\mathrm{H}$ were discussed in [25,26].

3. Hypernuclear cross section inferences

A global fit of the respective extracted yields was achieved in order to infer the cross sections of Λ, ${}^{3}_{\Lambda}\mathrm{H}$, and ${}^{4}_{\Lambda}\mathrm{H}$. The extracted raw yields without efficiency and acceptance corrections were already reported in [25]. The global fit was performed by means of a Bayesian approach based on the software framework BAT [27]. Within the BAT framework, the comparison between the data set $\vec{D}$ and the model $\mathcal{M}$, composed of the parameters of interest $\vec{\lambda}$ and of nuisance $\vec{\nu}$, assesses the complete posterior probability distribution of $\vec{\lambda}$ from the Bayes' Theorem:

$$P(\lambda_i|\vec{D}) \sim \int \mathcal{L}(\vec{D}|\vec{\lambda},\vec{\nu})\,\pi(\vec{\lambda},\vec{\nu})\,d\vec{\nu}d\vec{\lambda}_{i\neq j} \tag{1}$$

The posterior probability distributions are numerically calculated by Monte Carlo sampling: the Markov Chain Monte Carlo method of Metropolis-Hastings algorithm [28] implemented by the BAT framework [27]. In our case the parameters of interest are the cross sections, $\hat{\sigma}_i$, of Λ, ${}^{3}_{\Lambda}\mathrm{H}$, and ${}^{4}_{\Lambda}\mathrm{H}$ and the yield ratio, $\hat{Ratio}_{i/j}$, such as ${}^{3}_{\Lambda}\mathrm{H}/{}^{4}_{\Lambda}\mathrm{H}$, ${}^{3}_{\Lambda}\mathrm{H}/\Lambda$, and ${}^{4}_{\Lambda}\mathrm{H}/\Lambda$. By definition, the additional parameters of the likelihood model, presented later on, are considered as the nuisance parameters. The likelihood function used to calculate the marginalized posterior distribution functions of each parameter of interest was defined by:

$$\mathcal{L} = \prod_i \mathcal{N}(\hat{N}_i, N_{obs_i}, \sigma^2_{Nobs_i}) \times \prod_{ij} \mathcal{W}(\hat{R}_{ij}, N_{obs_i}, \sigma^2_{Nobs_i}, N_{obs_j}, \sigma^2_{Nobs_j}) \tag{2}$$

where N_{obs} and σ_{Nobs} correspond to the mean value and the 1-σ standard deviation of the estimated yield of the specie indexed by i, as reported in [25] and in Table 1. They constitute the data set $\vec{D}$. The probability density functions, $\mathcal{N}$ and $\mathcal{W}$, represent respectively the Gaussian distribution, and the ratio of two correlated normal random variables described in [29]. They model the cross sections and the yield ratios respectively to compare the nested estimators $\hat{N}_i$ and $\hat{R}_{ij}$ to the data set.

The nested estimator $\hat{N}_i$ is the yield obtained from the cross section estimator $\hat{\sigma}_i$ of the species of interest, Λ, ${}^{3}_{\Lambda}\mathrm{H}$, ${}^{4}_{\Lambda}\mathrm{H}$. The yield estimator $\hat{N}_i$ is defined as follows:

$$\hat{N}_i = \hat{\sigma}_i \cdot BR_i \cdot Eff_i \cdot Trig_i \cdot \mathfrak{L} \tag{3}$$

in which BR, Eff, $Trig$ and $\mathfrak{L}$ correspond to the branching ratio, the reconstruction and acceptance efficiency, the trigger system efficiency and the total integrated luminosity in μb^{-1}, respectively. Each of those parameters was considered and included into the likelihood function (2) as nuisance parameters modeled by different probability density functions in order to account for the systematic uncertainties and correlations of those parameters. The used branching ratio values are reported in Table 1 with their respective references.

Table 1
Summary of the parameter set used as input to the combined fit of the production cross section of the species Λ, ${}^{3}_{\Lambda}\mathrm{H}$, ${}^{4}_{\Lambda}\mathrm{H}$, and of the yield ratios ${}^{3}_{\Lambda}\mathrm{H}/{}^{4}_{\Lambda}\mathrm{H}$, ${}^{3}_{\Lambda}\mathrm{H}/\Lambda$, ${}^{4}_{\Lambda}\mathrm{H}/\Lambda$. The observable N_{obs} and σ_{Nobs} are extracted from the published results of the study of Λ, ${}^{3}_{\Lambda}\mathrm{H}$, ${}^{4}_{\Lambda}\mathrm{H}$ signals [25]. The branching ratio of Λ is obtained from [30] while the branching ratio of ${}^{3}_{\Lambda}\mathrm{H}$ and ${}^{4}_{\Lambda}\mathrm{H}$ are extracted from [31] and [32,33].

	Λ	${}^{3}_{\Lambda}\mathrm{H}$	${}^{4}_{\Lambda}\mathrm{H}$
N_{obs}	280	154	123
σ_{Nobs}	63	49	33
Branching ratio π^-/all	0.642	0.640	0.735
Branching ratio 2-body π^-/all π^-	1	0.379	0.690
Monte Carlo acceptance correction	0.142	1	1
TOF+ trigger efficiency	0.097	0.990	0.990
TOF+ trigger efficiency uncertainty	0.01	0.09	0.09
Secondary vertex trigger efficiency		0.51	
Vertex trigger efficiency uncertainty		0.05	
Luminosity		0.054 pb^{-1}	
Luminosity uncertainty		0.0011 pb^{-1}	

The acceptance and reconstruction efficiency of Λ, ${}^{3}_{\Lambda}\mathrm{H}$ and ${}^{4}_{\Lambda}\mathrm{H}$ species as a function of their decay length in the laboratory frame were used to correct the kinematics dependency of the measured yields within the experimental acceptance. In the case of Λ hyperon, its total production cross section was intended to be estimated since UrQMD theoretical calculations [34,35] are considered to model the Λ phase space reasonably [36–42]. Therefore, the phase space dependence within the experimental acceptance and reconstruction efficiency is first corrected, then the missing proportion of the Λ hyperon phase space is also corrected by the obtained value reported in Table 1 as *Monte Carlo acceptance correction*. In the case of ${}^{3}_{\Lambda}\mathrm{H}$ and ${}^{4}_{\Lambda}\mathrm{H}$ species, the acceptance and reconstruction acceptance is only corrected within the experimental acceptance since there is no validated theoretical models. Therefore, their production cross section is model independent, and in Table 1 a factor of 1 for their *Monte Carlo acceptance correction* is denoted.

Fig. 2 shows the acceptance and reconstruction efficiency as a function of the decay length in the laboratory frame and as function of the rapidity and Pt for Λ hyperon and ${}^{3}_{\Lambda}\mathrm{H}$ and ${}^{4}_{\Lambda}\mathrm{H}$ on the left and right panels respectively. The difference in the phase space distributions of the species of interests are fully included in the acceptance and reconstruction efficiency as a function of the decay length in the laboratory frame. In the inference of the cross sections and yield ratios, the acceptance and efficiency correction were applied via their decay length dependency in order to account for the lifetime estimation uncertainties. Those uncertainties were modeled by the lifetime probability density functions calculated from the likelihood functions obtained during lifetime extraction reported in [25].

The trigger efficiency combined the *TOF+* trigger and the secondary vertex trigger efficiency. The *TOF+* trigger efficiency was obtained by comparing the measured yields of isotopes detected by the TOF+ hodoscope wall between the minimum bias trigger and the hypernuclear accepted trigger. The low *TOF+* trigger efficiency for Λ hyperons reflects the specificity of trigger system that aimed to enhance the hypernuclear signal that includes a Helium isotope as decay fragment from others produced topologies like the Λ hyperon event. A systematic uncertainty was associated to the efficiency deviations when different parts of the data set were analyzed. The vertex trigger efficiency is the combination of the Monte Carlo simulation results of the trigger efficiency and the trigger rate study performed during the data taking. The trigger suppression rate of the vertex trigger setting was measured during the experiment. With the results of the Monte Carlo design study of vertex trigger, an extrapolation to the effective vertex trigger effi-

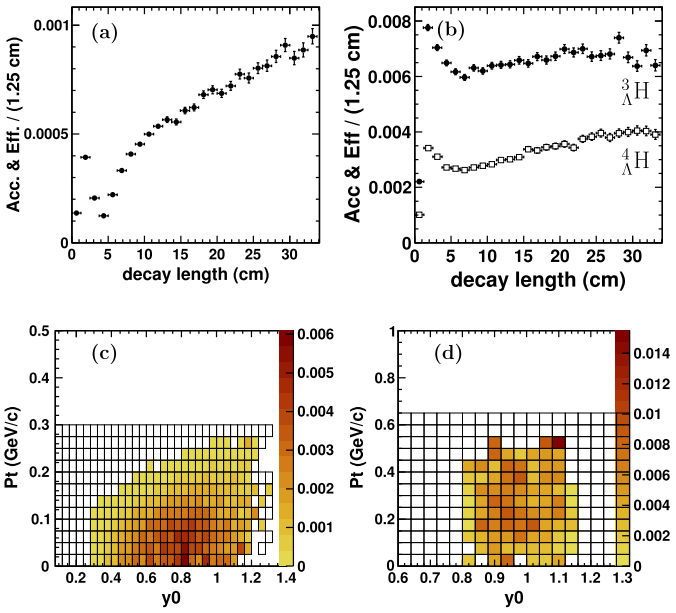

Fig. 2. (Color online.) Acceptance and reconstruction efficiency correction as a function of the decay length in the laboratory frame obtained via Monte Carlo simulations for Λ is shown in panel (a), and for the $^3_\Lambda$H and $^4_\Lambda$H hypernuclei are shown in panels (b) in black dot and open square respectively. The acceptance and reconstruction efficiency as functions of the kinetic variables $y0$ and Pt for Λ and the hypernuclear case are shown in panel (c) and (d) respectively. The open boxes shown in panel (c) and (d) represent to the phase space probed to estimate the efficiency as a function of $y0$ and Pt.

ciency was then deduced. A systematic uncertainty was associated to this extrapolation and the estimation procedure. Each trigger efficiency is modeled by a Gaussian density function to incorporate the systematic uncertainties of those efficiency estimations. The estimated parameters for the trigger efficiencies are reported in Table 1.

The total integrated luminosity was estimated with the help of the scaler detectors used to monitor the spill intensity over the data-taking period. Additionally, the integrated luminosity uncertainty is included in the calculation. The integrated luminosity and the estimation uncertainty are reported in Table 1.

The second nested estimator $\hat{R}_{ij}$ is defined as follows:

$$\hat{R}_{ij} = \hat{Ratio}_{i/j} \cdot \frac{BR_i \cdot Eff_i \cdot Trig_i}{BR_j \cdot Eff_j \cdot Trig_j} \tag{4}$$

where $\hat{Ratio}_{i/j}$ corresponds to the yield ratio such as: $^3_\Lambda$H/$^4_\Lambda$H, $^3_\Lambda$H/Λ, and $^4_\Lambda$H/Λ.

The marginalized posterior distributions of the parameters of interest are then calculated. The prior functions used for the parameters of interest were uniform priors. The summary of the values extracted from the posterior distribution functions is presented in Table 2. It includes the expected value and the standard deviation of those posterior distributions. In addition, the contribution from the systematic uncertainties of the efficiency corrections and luminosity estimations are also reported. The sensitivity of the interval estimation to the choice of prior distribution was also investigated and reported in the last column of Table 2.

4. Results and discussion

4.1. Cross sections and yield ratios

With the methods and procedures described above, the cross section values for Λ, $^3_\Lambda$H and $^4_\Lambda$H were deduced to be respectively 0.3 ± 0.1 (stat + sys + prior) mb, 3.9 ± 1.4 (stat + sys + prior) μb and 3.1 ± 1.0 (stat + sys + prior) μb within the experimental acceptance ($y0 > 0.32$ or $y_{lab} > 1.20$ as visible in Fig. 2). The reported 1-σ standard deviation will correspond to the combination of the statistical, systematic and prior uncertainties of Table 2. The deduced hypernuclear cross section values are restricted to the projectile rapidity region within the experimental acceptance. The total Λ cross section was estimated to be 1.7 ± 0.8 mb, with the correction of phase space acceptance of the UrQMD model calculation as explained in Section 3.

Table 2
Summary of the estimations of the parameters of interest such as the cross sections and the yield ratios. $\langle x \rangle$ and σ_{stat} correspond to the expected value and the statistical standard deviation of the posterior probability density function. σ_{sys} and σ_{prior} stand for the systematic uncertainties and the prior sensitivity uncertainties.

	$\langle x \rangle$	σ_{stat}	σ_{sys}	σ_{prior}
Λ_{tot} (mb)	1.7	± 0.7 (stat)	± 0.4 (sys)	± 0.2 (prior)
Λ_{obs} (mb)	0.3	± 0.1 (stat)	± 0.06 (sys)	± 0.03 (prior)
$^3_\Lambda$H (μb)	3.9	± 1.3 (stat)	± 0.3 (sys)	± 0.3 (prior)
$^4_\Lambda$H (μb)	3.1	± 1.0 (stat)	± 0.3 (sys)	± 0.1 (prior)
$^3_\Lambda$H/$^4_\Lambda$H	1.4	± 0.7 (stat)	± 0.1 (sys)	± 0.2 (prior)
$^3_\Lambda$H/Λ ($\times 10^{-3}$)	2.6	± 1.4 (stat)	± 0.3 (sys)	± 0.2 (prior)
$^4_\Lambda$H/Λ ($\times 10^{-3}$)	2.1	± 1.1 (stat)	± 0.1 (sys)	± 0.2 (prior)

The inferred total cross section of Λ can be compared to published experimental estimations. Thanks to the Glauber model calculation [43–45], an estimation of the Λ total cross section for the ^{6}Li + ^{12}C reaction can be obtained from the proton–proton cross section at the excess energy of 204 MeV and 239 MeV measured by the COSY-TOF Collaboration [46]. The deduced value is 1.5 ± 0.1 mb, which within errors agrees with our measured total production cross section of Λ hyperon. Cross section values of $^3_\Lambda$H and $^4_\Lambda$H are of the order of μb, similar to the values calculated by Gaitanos et al. [22].

The yield ratio $^3_\Lambda$H/$^4_\Lambda$H of 1.4 ± 0.8 was also inferred and can be compared to the theoretical estimation value of 4.3 obtained by Botvina et al. [24]. While the experimental and theoretical estimation are close, additional consideration in the theoretical calculations of Botvina et al. will be necessary in order to reproduce the experimental inference. The ratio of cross section values for $^3_\Lambda$H and $^4_\Lambda$H with respect to that for Λ is $(2.6 \pm 1.4) \times 10^{-3}$ and $(2.1 \pm 1.1) \times 10^{-3}$, respectively. Yet no theoretical prediction of those ratios are available for direct comparison.

Additionally the double ratios $S_3 = {}^3_\Lambda\mathrm{H}/{}^3\mathrm{He} \cdot \mathrm{p}/\Lambda$ and $S_4 = {}^4_\Lambda\mathrm{H}/{}^4\mathrm{He} \cdot \mathrm{p}/\Lambda$ so-called Strangeness Population Factor [15,16,47] were determined. From a set of 5×10^5 reconstructed minimum bias events, the yield ratios p/^{3}He and p/^{4}He were evaluated with efficiency and acceptance corrected to be 19.1 ± 0.5 and 5.7 ± 0.1 respectively. Therefore within the phase space acceptance of the experiment, S_3 and S_4 were estimated to be 0.28 ± 0.14 and 0.08 ± 0.04 respectively. Those estimations can be compared to the ones of [15] and show a good agreement. The trend of the theoretical calculation on the ratio S_3 [47] can be extrapolated to $\sqrt{s_{NN}} = 2.70$ GeV and shows a fair agreement with the obtained value. The implications of those new available values have to be theoretically assessed.

4.2. Multiplicities, rapidity and Pt distributions

The multiplicity of hypernuclei per collision was also calculated considering a total reaction cross section of 667 ± 33 mb. The total reaction cross section was evaluated with the help of Glauber model calculations [43–45] assuming the inelastic pp cross section of 27 ± 1 mb at the kinetic energy of 2.0 GeV [48]. The total Λ multiplicity per collision is then of $2.6 \pm 1.2 \times 10^{-3}$, and the mul-

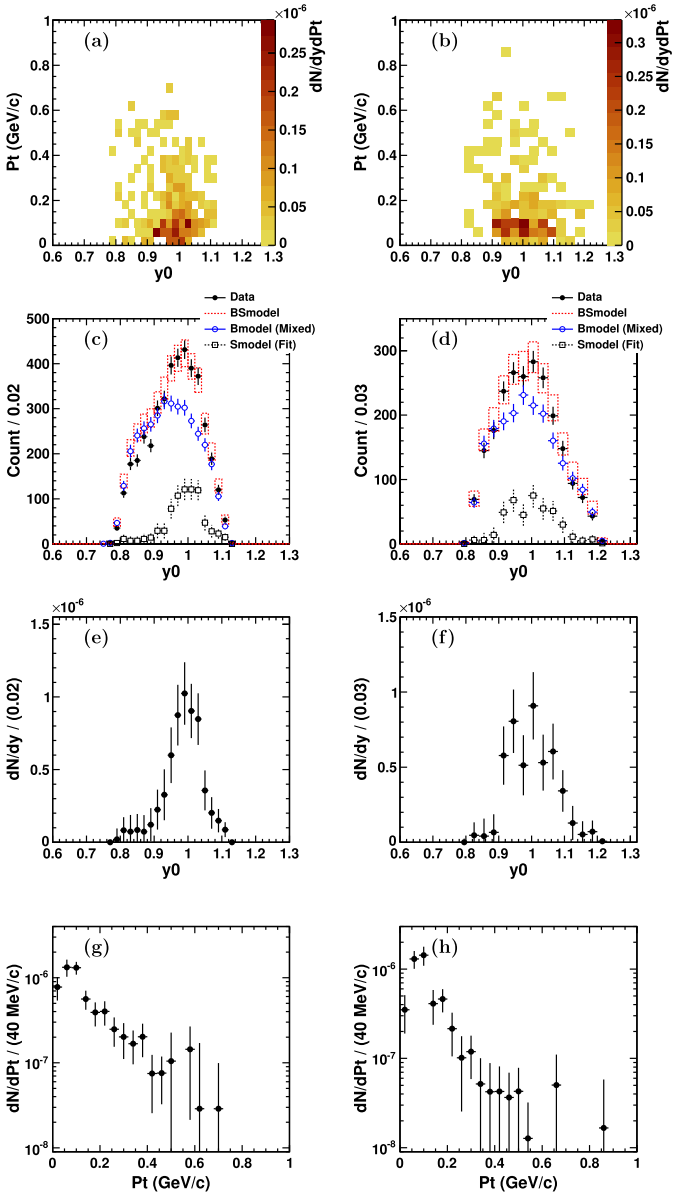

Fig. 3. (Color online.) Multiplicity distribution as a function of the rapidity observable $y0$ and of the transversal momentum Pt in the center-of-mass system for ${}^{3}_{\Lambda}\mathrm{H}$ in panel (a), ${}^{4}_{\Lambda}\mathrm{H}$ in panel (b), respectively. In panels (c) and (d) the projected rapidity distributions of the data set ${}^{3}_{\Lambda}\mathrm{H}$ and ${}^{4}_{\Lambda}\mathrm{H}$ respectively are shown in black full circle together with extracted signal contribution *Smodel* (open box), the background-only distribution from the mixed event analysis *Bmodel* (open circle) and the signal-plus-background model *BSmodel* (dash box representing the 1-σ standard deviation interval). Panels (e), (f) and (g), (h) show the rapidity and Pt distribution of extracted ${}^{3}_{\Lambda}\mathrm{H}$ and ${}^{4}_{\Lambda}\mathrm{H}$ signal, respectively.

tiplicities of the ${}^{3}_{\Lambda}\mathrm{H}$ and ${}^{4}_{\Lambda}\mathrm{H}$ hypernuclei are $5.8 \pm 2.1 \times 10^{-6}$, and $4.6 \pm 1.6 \times 10^{-6}$, respectively.

The multiplicity distributions of ${}^{3}_{\Lambda}\mathrm{H}$ and ${}^{4}_{\Lambda}\mathrm{H}$ signal as a function of the rapidity in the center-of-mass system, $y0$, and transversal momentum, Pt, are then shown in top panels of Fig. 3. The hypernuclear signal was extracted from the experimental data set and the mixed event data set of $y0 - Pt$ observables. The bins size of data sets were 40 MeV/c in Pt and 0.02 and 0.03 unit of $y0$ for ${}^{3}_{\Lambda}\mathrm{H}$ and ${}^{4}_{\Lambda}\mathrm{H}$ respectively. For each bin, the signal contribution was estimated by a maximum likelihood ratio method from the background contribution (mixed event) and the signal-plus-background contribution (experimental data). For each extracted signal distribution shown in Fig. 3, the acceptance and reconstruction efficiency dependency were corrected as function of the Pt since the $y0$ dependency is fairly uniform within the experimental acceptance as shown in the panel (d) of Fig. 2.

The panels (c) and (d) of Fig. 3 show the projected rapidity distribution of the data set with the following distributions: the extracted signal (*Smodel*), the background-only model from the mixed event analysis (*Bmodel*) and the signal-plus-background contribution (*SBmodel*). The last four panels of Fig. 3, show the projected rapidity $y0$ and Pt distribution of the extracted signal for ${}^{3}_{\Lambda}\mathrm{H}$ and ${}^{4}_{\Lambda}\mathrm{H}$ hypernuclei on the left- and right-hand side, respectively. The mean value and standard deviation of the rapidity distribution of ${}^{3}_{\Lambda}\mathrm{H}$ and ${}^{4}_{\Lambda}\mathrm{H}$ are respectively $\langle y0 \rangle = 0.98 \pm 0.01$, $\sigma_{y0} = 0.06 \pm 0.01$ and $\langle y0 \rangle = 1.00 \pm 0.01$, $\sigma_{y0} = 0.07 \pm 0.01$. One can remark that the experimental rapidity distribution ${}^{3}_{\Lambda}\mathrm{H}$ and ${}^{4}_{\Lambda}\mathrm{H}$ falls within the Monte Carlo experimental acceptance shown in Fig. 2. Moreover the multiplicity density decrease in the rapidity region $[0.8; 0.9]$ shown in the ${}^{3}_{\Lambda}\mathrm{H}$ and ${}^{4}_{\Lambda}\mathrm{H}$ rapidity distribution represents a physical upper limit since it is still within the experimental acceptance.

5. Conclusion

Those experimental estimations of the production cross section for Λ hyperon, ${}^{3}_{\Lambda}\mathrm{H}$ and ${}^{4}_{\Lambda}\mathrm{H}$ hypernuclei and the respective yield ratio ${}^{3}_{\Lambda}\mathrm{H}/{}^{4}_{\Lambda}\mathrm{H}$, ${}^{3}_{\Lambda}\mathrm{H}/\Lambda$ and ${}^{4}_{\Lambda}\mathrm{H}/\Lambda$, will allow to restrain several theoretical parameters of the hyper-matter production models in the projectile rapidity region for the first time. The important theoretical parameters describing the hyper-matter production are the coalescence factor [22,49], the spectator excitation energy [24] and temperature [23]. Moreover the dynamics of the reaction [22,4,5] or the time window of interaction between the participant and spectators [50,51] depends strongly on those yield ratios and hypernuclear production cross section. Until now, those current theoretical models do not use the experimental data as validation since no experimental data were available. The transport models for the hyper-matter dynamics will be constrained by the reported multiplicities, rapidity and Pt distributions. Indeed the rapidity and Pt distributions of ${}^{3}_{\Lambda}\mathrm{H}$ and ${}^{4}_{\Lambda}\mathrm{H}$ hypernuclei are sensitive to their dynamical formation and therefore of the pre-equilibrium phase of the collision. It will allow better theoretical predictions of the hypernuclear production in other collisions and at different energies that will happen in the future facilities such as FAIR, NICA or J-PARC.

In conclusion, the estimations of the production cross section of ${}^{3}_{\Lambda}\mathrm{H}$ and ${}^{4}_{\Lambda}\mathrm{H}$ of 3.9 ± 1.4 µb and 3.1 ± 1.0 µb respectively in the projectile rapidity region were performed by a combined fit based on a Bayesian approach. Additionally the total production cross section of 1.7 ± 0.8 mb for Λ hyperon was estimated during the combined inference. Production ratios of ${}^{3}_{\Lambda}\mathrm{H}/{}^{4}_{\Lambda}\mathrm{H}$, ${}^{3}_{\Lambda}\mathrm{H}/\Lambda$ and ${}^{4}_{\Lambda}\mathrm{H}/\Lambda$ of 1.4 ± 0.8, $2.6 \pm 1.4 \times 10^{-3}$ and $2.1 \pm 1.1 \times 10^{-3}$ respectively were also deduced. The factors S_3 and S_4 of 0.28 ± 0.14 and 0.08 ± 0.04 respectively were as well determined. The total multiplicity per collision of $2.6 \pm 1.2 \times 10^{-3}$ for Λ hyperon was inferred, while the hypernuclear multiplicity in the projectile rapidity region of $5.8 \pm 2.1 \times 10^{-6}$ and $4.6 \pm 1.6 \times 10^{-6}$ for respectively ${}^{3}_{\Lambda}\mathrm{H}$ and ${}^{4}_{\Lambda}\mathrm{H}$. Those cross section estimations will validate theoretical models of the production of hypernuclear matter in heavy ion collisions. It will allow to obtain a more precise description of the reaction mechanism and of the dynamics between the participant and spectator region.

Acknowledgements

The authors would like to thank the GSI Departments of Accelerator, of Experimental Electronics, of the Detector Laboratory and

of the Target Laboratory and the Electronics Department of the Institute for Nuclear Physics of Mainz University for supporting the project. The HypHI project is funded by the Helmholtz Association as Helmholtz-University Young Investigators Group VH-NG-239 at GSI, and the German Research Foundation (DFG) under contract number SA 1696/1-1. The authors acknowledge the financial support provided by the Ministry of Education, Science and Culture of Japan, Grant-in-Aid for Scientific Research on Priority Areas 449, and Grant-in-Aid for promotion of Cooperative Research in Osaka Electro-Communication University (2004–2006). This work is also supported by the Ministry of Education, Science and Culture of Japan, Grants-in-Aid for Scientific Research 18042008 and EU FP7 Hadron-Physics-2 SPHERE. A part of this work was carried out on the HIMSTER high performance computing infrastructure provided by the Helmholtz-Institute Mainz. We would also like to thank to A. Botvina, T. Gaitanos, and H. Lenske for the involved discussions.

References

[1] J. Aichelin, Phys. Rep. 202 (1991) 233.
[2] H. Weber, E.L. Bratkovskaya, W. Cassing, H. Stöcker, Phys. Rev. C 67 (2003) 014904.
[3] X. Lopez, Prog. Part. Nucl. Phys. 53 (2004) 149.
[4] A.S. Botvina, J. Pochodzalla, Phys. Rev. C 76 (2007) 024909.
[5] A.S. Botvina, K.K. Gudima, J. Steinheimer, M. Bleicher, I.N. Mishustin, Phys. Rev. C 84 (2011) 064904.
[6] R. Barth, P. Senger, W. Ahner, P. Beckerle, C. Bormann, D. Brill, M. Cieślak, M. Dębowski, E. Grosse, P. Koczoń, et al., KaoS Collaboration, Phys. Rev. Lett. 78 (1997) 4007.
[7] P. Moskal, et al., J. Phys. G 28 (2002) 1777.
[8] A.K. Kerman, M.S. Weiss, Phys. Rev. C 8 (1973) 408–410.
[9] K. Nield, et al., Phys. Rev. C 13 (1976) 1263.
[10] A.U. Abdurakhimov, et al., Nuovo Cimento A 102 (1989) 645.
[11] S. Avramenko, et al., Nucl. Phys. A 547 (1992) 95c.
[12] F. Asai, H. Bando, M. Sano, Phys. Lett. B 145 (1984) 19.
[13] M. Wakai, H. Bando, M. Sano, Phys. Rev. C 38 (1988) 748.
[14] H. Bando, M. Sano, J. Zofka, M. Wakai, Nucl. Phys. A 501 (1989) 900.
[15] T.A. Armstrong, et al., Phys. Rev. C 70 (2004) 024902.
[16] STAR-Collaboration, Science 328 (2010) 58.
[17] Y.-G. Ma, STAR Collaboration, EPJ Web Conf. 66 (2014) 04020.
[18] R. Lea, ALICE Collaboration, Nucl. Phys. A 914 (2013) 415.
[19] N. Martin, ALICE Collaboration, Nucl. Phys. A 931 (2014) 1103.
[20] P. Braun-Munzinger, K. Redlich, J. Stachel, arXiv:nucl-th/0304013, 2003.
[21] A. Andronic, P. Braun-Munzinger, J. Stachel, H. Stocker, Phys. Lett. B 697 (2011) 203.
[22] T. Gaitanos, H. Lenske, U. Mosel, Phys. Lett. B 675 (2009) 297.
[23] V. Topor Pop, S. Das Gupta, Phys. Rev. C 81 (2010) 054911.
[24] A.S. Botvina, I.N. Mishustin, J. Pochodzalla, Phys. Rev. C 86 (2012) 011601.
[25] C. Rappold, et al., Nucl. Phys. A 913 (2013) 170.
[26] C. Rappold, et al., Phys. Lett. B 728 (2014) 543.
[27] A. Caldwell, D. Kollár, K. Kröninger, Comput. Phys. Commun. 180 (2009) 2197.
[28] N. Metropolis, A.W. Rosenbluth, M.N. Rosenbluth, A.H. Teller, E. Teller, J. Chem. Phys. 21 (1953) 1087.
[29] D.V. Hinkley, Biometrika 56 (1969) 635.
[30] J. Beringer, et al., Phys. Rev. D 86 (2012) 010001.
[31] H. Kamada, J. Golak, K. Miyagawa, H. Witala, W. Glöckle, Phys. Rev. C 57 (1998) 1595.
[32] H. Outa, et al., Nucl. Phys. A 639 (1998) 251c.
[33] M. Juric, et al., Nucl. Phys. B 52 (1973) 1.
[34] S. Bass, M. Belkacem, M. Bleicher, M. Brandstetter, L. Bravina, et al., Prog. Part. Nucl. Phys. 41 (1998) 255.
[35] M. Bleicher, E. Zabrodin, C. Spieles, S.A. Bass, C. Ernst, S. Soff, L. Bravina, M. Belkacem, H. Weber, H. Stöcker, et al., J. Phys. G, Nucl. Part. 25 (1999) 1859.
[36] M. Merschmeyer, Ph.D. thesis, University of Heidelberg, 2004, 104 pp.
[37] H. Petersen, M. Bleicher, S.A. Bass, H. Stocker, arXiv:0805.0567, 2008.
[38] E. Bratkovskaya, M. Bleicher, W. Cassing, M. van Leeuwen, M. Reiter, et al., Prog. Part. Nucl. Phys. 53 (2003) 225.
[39] E.L. Bratkovskaya, M. Bleicher, M. Reiter, S. Soff, H. Stöcker, M. van Leeuwen, S.A. Bass, W. Cassing, Phys. Rev. C 69 (2004) 054907.
[40] K. Dey, B. Bhattacharjee, Phys. Rev. C 89 (2014) 054910.
[41] N. Abgrall, Aduszkiewicz, et al., NA61/SHINE Collaboration, Phys. Rev. C 89 (2014) 025205.
[42] G. Agakishiev, O. Arnold, A. Balanda, D. Belver, A. Belyaev, J. Berger-Chen, A. Blanco, M. Böhmer, J. Boyard, P. Cabanelas, et al., Eur. Phys. J. A (ISSN 1434-6001) 50 (2014).
[43] B. Alver, M. Baker, C. Loizides, P. Steinberg, arXiv:0805.4411, 2008.
[44] C. Loizides, J. Nagle, P. Steinberg, arXiv:1408.2549, 2014.
[45] W. Broniowski, M. Rybczyński, P. Bożek, Comput. Phys. Commun. 180 (2009) 69.
[46] M. Abdel-Bary, S. Abdel-Samad, K.-T. Brinkmann, H. Clement, J. Dietrich, E. Doroshkevich, S. Dshemuchadse, K. Ehrhardt, A. Erhardt, W. Eyrich, et al., Eur. Phys. J. A 46 (2010) 27.
[47] S. Zhang, J. Chen, H. Crawford, D. Keane, Y. Ma, Z. Xu, Phys. Lett. B (ISSN 0370-2693) 684 (2010) 224.
[48] C. Lechanoine-LeLuc, F. Lehar, Rev. Mod. Phys. 65 (1993) 47.
[49] J. Steinheimer, K. Gudima, A. Botvina, I. Mishustin, M. Bleicher, H. Stöcker, Phys. Lett. B 714 (2012) 85.
[50] C. Dorso, J. Randrup, Phys. Lett. B 301 (1993) 328.
[51] R.K. Puri, J. Aichelin, J. Comput. Phys. 162 (2000) 245.